NUCL SCI TECH (2016) 27:85
DOI 10.1007/s41365-016-0079-5

Activation and shutdown dose-rate analyses for the EAST NBI test facility

Yu-Qing Chen[1] · Ji Wang[1] · Bin Wu[1] · Jun Li[1] · Ya-Hong Xie[1] · Guo-Qiang Zhong[1] · Chun-Dong Hu[1]

Received: 15 March 2015 / Revised: 2 June 2015 / Accepted: 2 June 2015 / Published online: 8 July 2016

Abstract An analysis of the neutron activation and shutdown dose rates was performed for the EAST high-power deuterium neutral beam injector test facility (EAST NBITF) by using the multiparticle transport code FLUKA 2011.2. Also, the neutron and neutron-induced gamma spectra of the facility's vacuum vessel were evaluated. The results identified the major radionuclides ^{99}Mo, ^{65}Ni, ^{58}Co, ^{56}Mn, and ^{51}Cr for the vacuum vessel and the primary nuclide ^{64}Cu for both the ion dump and the calorimeter. The simulated results indicated that, when the EAST NBITF operates within the design parameters of deuterium energy 80 keV, current 50 A, and pulse 100 s, the neutron intensity will achieve 10^{11} n/s with no radiation safety problems after the EAST NBITF shuts down.

Keywords Shutdown dose rate · Neutron activation · Radionuclides

1 Introduction

To raise plasma temperature and initiate sustained fusion, high-power deuterium neutral beam injectors (NBIs), including JET, TFTR, and DIIID, have become an important auxiliary heating method. The Experimental Advanced Superconducting Tokomak has also developed the first neutral beam injection system (NBIS). To test the performance of the EAST NBI, a test facility (EAST NBITF) was constructed.

When the EAST NBITF operates, large sections of the energetic beam ion are stopped by both the ion dump and the calorimeter (approximately 80 %) along the beam line, and neutrons are produced via D(d,n)3He reaction [1–5]. Calculations of neutron production demonstrate that the calorimeter is the main neutron source [6–8].

These neutrons activate the components for the EAST NBITF and cause the material deterioration of the properties [2, 8–11]. After NBITF shutdown, these neutron-induced photons become a physical health concern for maintenance and repair workers. However, the neutron activation and shutdown rates of EAST NBITF have not been analyzed. This paper focuses on neutron activation and dose rates simulated by FLUKA 2011.2 code, a multiparticle transport code widely applied in radiation protection studies [12–14].

2 Geometrical model

To evaluate neutron transport in the EAST NBITF structure, a geometric model, the 2D EAST NBITF, was implemented into FLUKA code. The model, shown in Fig. 1, contains all the critical components: beam source,

This work was supported by the International S&T Cooperation Program of China (No. 2014DFG61950), National Magnetic Confinement Fusion Science Program (No. 2013GB101001), and the National Natural Science Foundation of China (No. 11405207).

✉ Ji Wang
wangji@ipp.ac.cn

Yu-Qing Chen
chenyq205@ipp.ac.cn

[1] Institute of Plasma Physics, Chinese Academy of Sciences, Hefei 230031, China

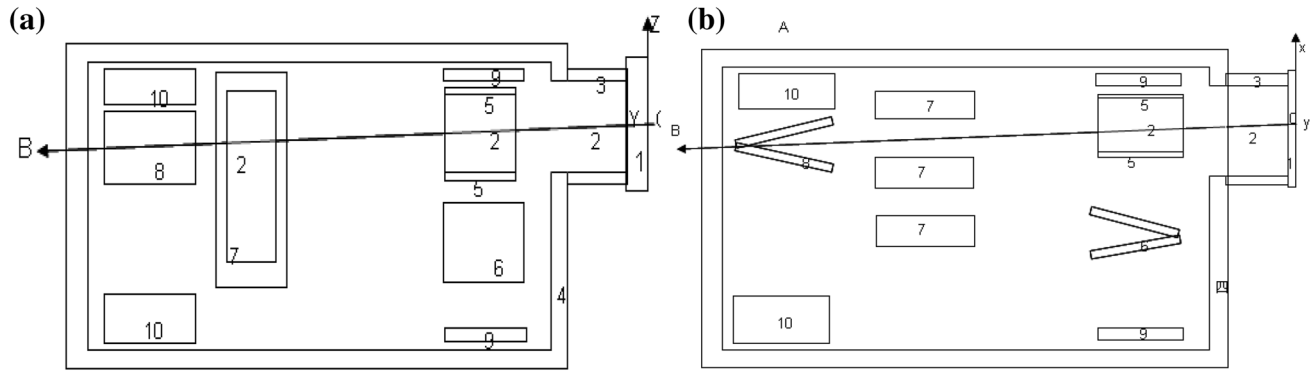

Fig. 1 NBI geometric model **a** side view of NBI and **b** top view of NBI

neutralizer, residual ion dump (RID), calorimeter, cryopanel, and vacuum vessel (VV). The ion source consists of rectangular parallelepipeds 125 cm long, 66 cm high, and 45 cm wide. For the beamline component, the VV had a cylindrical shape, approximately 1.5 cm thick. The neutralizer is a box [15].

The calorimeter consisted of two slab vertical parallelepiped panels, which formed an 11° angle from the top view. Each panel was 240 cm long, 200 cm wide, and 5 cm thick, and the RID had the same structure. The EAST NBITF had a total length of 5.25 m. The components of the geometrical model and the material compositions are listed in Table 1.

3 Mathematical method theory

3.1 Neutron-intensity calculations

During deuterium operation of EAST NBITF, the deuterium ions were produced and accelerated by the ion source, and the largest part of the beam power was impinged onto the ion dump and the calorimeter (approximately 80 %). The neutrons were produced in the same manner as with the drive-in solid-target neutron sources. Therefore, the calorimeter serves as the main neutron source. To calculate neutron intensity, the adopted model assumes that the deuteron beam, with initial energy, E_0, and the current density, I, normally occur on the planar surface of the calorimeter target (a similar method is used for the RID). A theoretical method of neutron intensity for high-energy deuterons stopped by a metal target was given by Kim [3–6]:

$$y = \frac{I_b}{e}\sum_{i=1}^{3} if_i \int_0^R \sigma(E(x)/i)C_{iD}(x,\theta)\mathrm{d}x \quad (1)$$

I_b is the total beam current; i is the number of nuclei per ion; f_i is the fraction of each ion species; and $E(x)$ is the particle energy at depth x. $\sigma[E(x)]$ is the cross section; and $C_D(x,\theta)$ is the saturation deuterium concentration (cm^{-3}) in the target. $\theta = D_{diff}t/R^2$ is calculated with the diffusion

Table 1 Regions and materials of the components

Regions	Components	Compositions (wt%)	Density (g/cm^3)
1. Arc chamber	Cu	100	8.96
2. Vacuum	Vacuum		
3. Vacuum vessel	SS316	C, 0.041; Si, 0.507; P, 0.023; S, 0.015; Cr, 17; Mn, 1.014; Fe, 66.9; Ni, 12; Mo, 2.5	8.0
4. Beamline vessel	SS316	C, 0.041; Si, 0.507; P, 0.023; S, 0.015; Cr, 17; Mn, 1.014; Fe, 66.9; Ni,12; Mo, 2.5	
5. Neutralizer	Cu	100	8.96
6. Ion dump	Cu	100	8.96
7. Bending magnet	Cu Fe	Cu, 50; Fe, 50	8.96
8. Calorimeter	Cu	100	8.96
9. Front cryopanel	Al	100	2.70
10. Rear cryopanel	Al	100	2.70
11. Environment	Air	C, 0.0124; N, 75.5268, 023.1781; Ar, 1.2827	1.205×10^{-3}

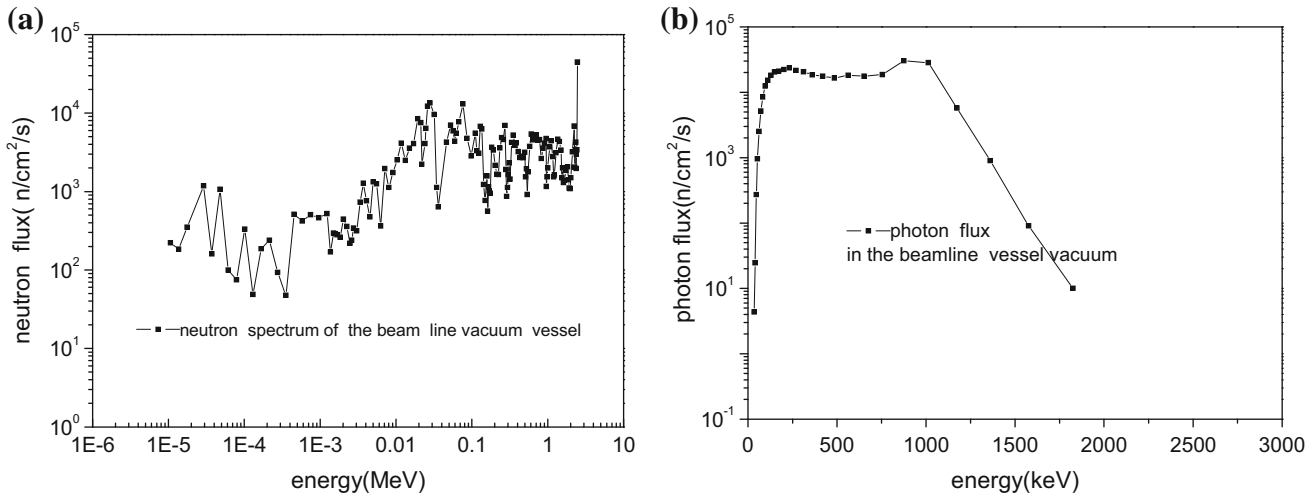

Fig. 2 Energy spectrum distribution: **a** neutron and **b** gamma

Table 2 Activities of vacuum vessels through different methods

Nuclide	Reaction	Theoretical value (Bq/kg)	FLUKA (Bq/kg)
^{99}Mo	^{98}Mo(n,γ)^{99}Mo	5.44E+06	7.88E+06
^{93}Mo	^{92}Mo(n,γ)^{93}Mo	5.02E+00	4.49E+00
^{65}Ni	^{64}Ni(n,γ)^{65}Ni	6.52E+06	1.17E+06
^{58}Co	^{58}Ni(n,p)^{58}Co	4.14E+05	1.36E+06
^{55}Fe	^{54}Fe(n,γ)^{55}Fe	7.52E+04	4.01E+04
^{56}Mn	^{55}Mn(n,γ)^{56}Mn	1.41E+08	7.28E+07
^{54}Mn	^{54}Fe(n,p)^{54}Mn	2.40E+05	1.37E+05
^{51}Cr	^{50}Cr(n,γ)^{51}Cr	5.52E+05	4.37E+05

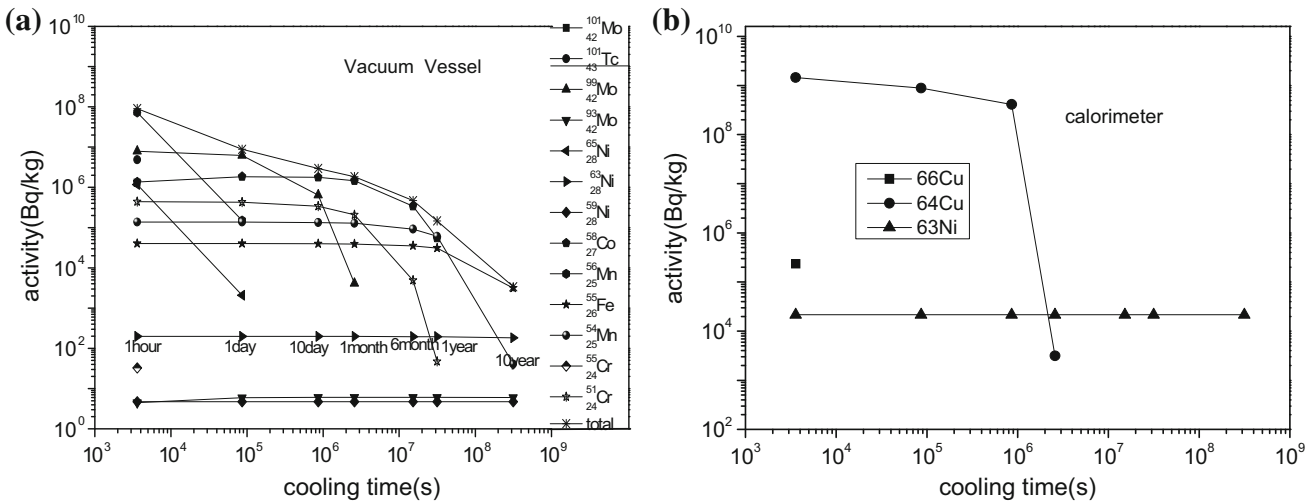

Fig. 3 Activities versus cooling times: **a** vacuum vessel activity and **b** calorimeter activity

coefficient D_{diff}, the pulse time t, and the beam ion stopping range R. Through the use of Eq. (1), the calculated neutron intensity for the calorimeter was 1.64×10^{10} n/s/A during the EAST NBITF running with the parameters 80 keV and 50 A and a pulse of 10–100 s [16]. The simulations indicate that the neutron intensity from D(T,p)4He was lower than that from D(d,n)3He by approximately five orders of magnitude [6, 15]. Therefore,

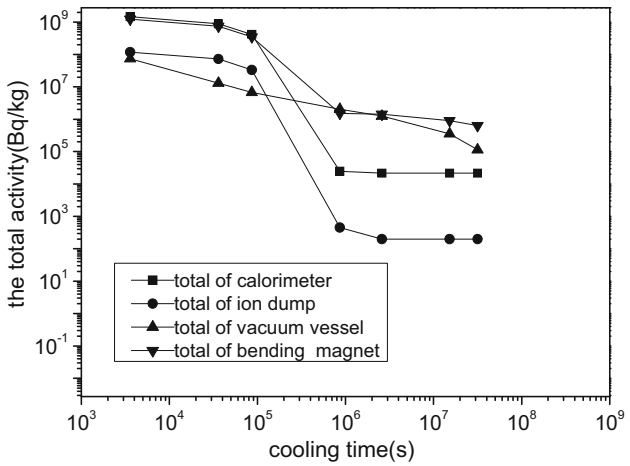

Fig. 4 Total activity versus cooling time

the D T neutron was omitted from neutron-activation analysis for this paper.

3.2 Activation calculations

The process of 2.45 MeV neutron activation is (n,γ) reaction. The cross sections of activation greatly heighten at low neutron energies (at most, only a few electron volts). With the distribution of neutron spectra, the number of radionuclides in a given material can be acquired by Eq. (2) [14]:

$$A_i = \phi_n \sum_{j \neq i} \sigma_{ij} n_{jt} \theta_{jt} \left(1 - \mathrm{e}^{-\lambda_i t_{\mathrm{irra}}}\right) \mathrm{e}^{-\lambda_i t_c}. \quad (2)$$

λ_i is the decay constant of the nuclide i; ϕ_{n} is the neutron flux (n/cm^2/s); σ_{ij} is the reaction cross section for reaction on producing i (cm^2); n_{jt} is the density of nuclide j in the target material (n/cm^3); t_c is the cooling time; t_{irra} is the irradiation time (can be considered effective time of EAST NBITF operating); and θ_{jt} is abundance of the i nuclide isotope in nature.

4 Results

4.1 Neutron and gamma spectra

To obtain the material activation and shutdown dose rate, it was necessary to analyze the neutron and photon spectra. Workers are first to exposed to the VV after a facility shutdown. Also, the material (SS316) is easily activated. The energy spectra of the VV are simulated through FLUKA 2011.2 in Fig. 2a, b. Because the effect of neutron scattering is significant [17–19], it can be included with the low-bias card in FLUKA.

Figure 2a reveals that the 2.45 MeV neutron intensity is still high after penetrating the calorimeter and cyropanel. Figure 2b shows the neutron-induced photon flux. During input of the neutron and photon spectra by the source card, the material activation can be simulated in the VV.

4.2 Activity analysis for NBI material

Through the use of Eq. (2), neutron activation can be evaluated for different irradiation times. To verify the reliability of the FLUKA code program, the values from Eq. (2) and FLUKA are compared with both the operating time (100 s) and the cooling time (1 h). Table 2 lists the activities of the material 1 h after shutdown. Deviations between Eq. (2) and FLUKA are 10× or fewer, which indicates the reliability of the values derived from FLUKA 2011.2.

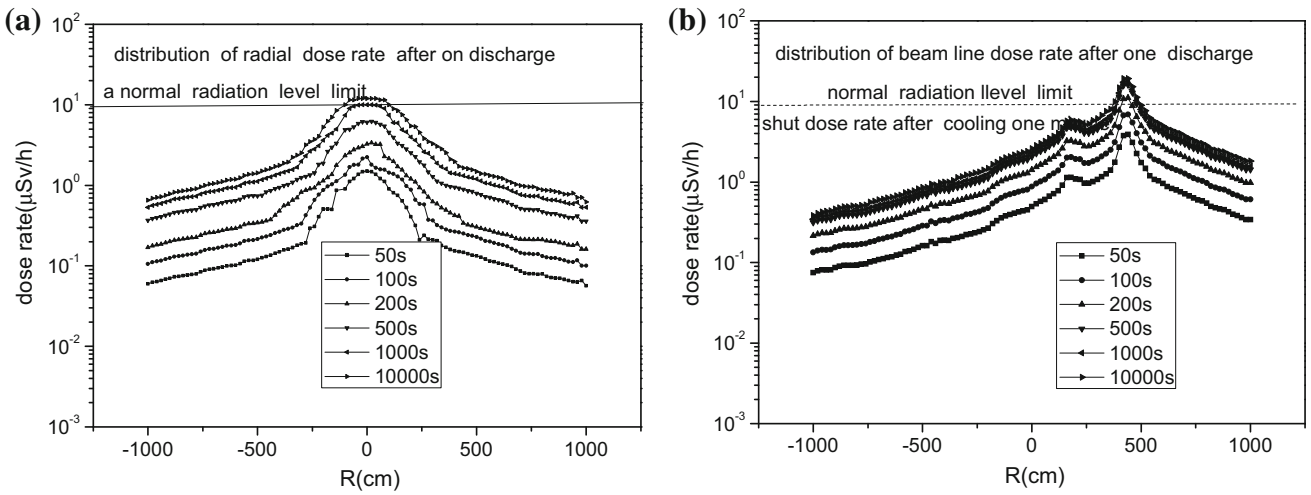

Fig. 5 Dose rates versus distance: **a** shutdown dose-rate distribution in the vertical direction and **b** shutdown dose-rate distribution along the beamline

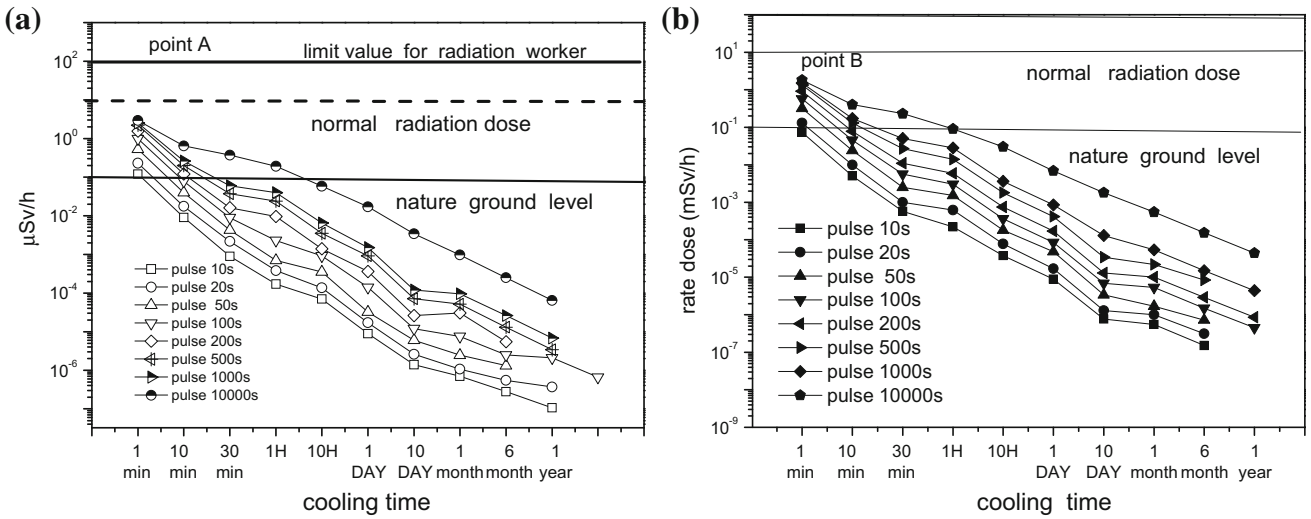

Fig. 6 Dose rate versus cooling time: **a** point A dose-rate distribution away from the vacuum vessel, 50 cm in the vertical direction and **b** point B dose-rate distribution away from vacuum vessel, 50 cm in the beam line direction

Figure 3 gives the functions between the activities of the NBI key components and the cooling times. In the VV, ^{99}Mo, ^{58}Co, ^{55}Fe, and ^{54}Mn are the dominant nuclei after 1 day of cooling time. The activities of the VV subside slowly after 10 days of cooling because the primary activities were the long half-lives of the decaying nuclei ^{55}Fe ($T_{1/2}$, 2.73 years); ^{99}Mo ($T_{1/2}$, 65.94 h); ^{51}Cr ($T_{1/2}$, 27.25 days); and ^{58}Co ($T_{1/2}$, 70.86 days). For the main radiation source calorimeter, ^{64}Cu ($T_{1/2}$, 12.7 h) had the shortest decaying half-life, and the activities of the ion calorimeter declined by six orders of magnitude after 10 days of cooling. However, the activity of calorimeter was higher than that of the VV during the initial cooling time.

Figure 4 shows the activities of the NBITF key components. Because the material and the neutron flux differ, the variation rules between total activity and cooling time are not same. Figure 4 indicates that neutron spectrum, neutron flux, target material, and cooling time affect the activities of the different components.

4.3 Shutdown dose rate of NBI

Neutron-induced photons are a major source of radiation after a NBITF shutdown. The dose rates can be obtained by multiplying the fluxes of the neutron/photon by the conversion factors of the flux-to-dose rate. The shutdown dose rates were analyzed in detail, and Fig. 5a and b demonstrates that the dose rates vary with distance after one pulse of discharge at 50–1000 s and after 1 min of cooling, with parameters of energy 80 keV and current 50 A. The shutdown dose rates rise as the length of the discharge pulse increases. Along the radial direction, the dose rates decrease away from the center of the deuterium beam. When the beamline direction was followed, the highest dose rates were 5.5 μSv/h at the calorimeter (R = 420 cm) with a pulse of 100 s because the calorimeter, situated there, was the main neutron source. Figure 5 demonstrates that the dose rates for pulses between 50–200 s (10μSv/h) fall below the safety standards of according to the ITER design rules [20]. The dose-rate limits for spot staff, occupational radiation workers, and the natural background are 10, 100, and 0.1 μSv/h, respectively.

The place away from the VV, approximately 50 cm, is the passageway for NBITF workers. Therefore, Fig. 6a, b shows the shutdown dose rates with different pulses. These simulations indicate that maintenance or repair staff can enter the hall at least 10 min after shutdown, when the pulse length extends 500 s after one discharge.

In many cases, multipulse discharge is a necessary attribute of the diagnostics schemes. The condition was simulated for pulse lengths of 100 s (the design pulse) with 10 pulses. The interval time between two pulses was 10 min. Compared with single-pulse discharge, the results (described in Fig. 7) were one magnitude of order lower because the multiple pulse intervals can cool the target. Therefore, the maximum shutdown dose rate is associated with pulses, cooling times, distance from the main neutron source, and material property.

5 Conclusion

FLUKA code was used to assess neutron activation for the key components of the EAST NBITF system, with operating the parameters of energy 80 keV, current 50 A, and pulses of 50–1000 s, respectively. In addition, the

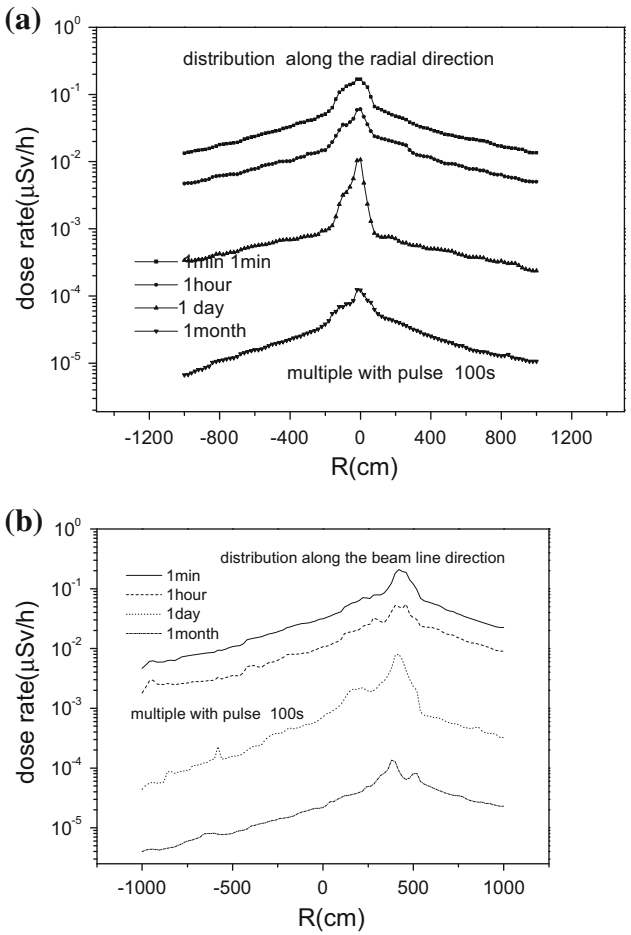

Fig. 7 Dose rate versus distance at different cooling time after multiple discharges for pulses of 100 s: **a** dose-rate distribution along the radial direction and **b** dose-rate distribution along the beam line direction

distributions of the neutron and the photon spectra of VV were simulated. Finally, the shutdown dose rates were analyzed after differential pulse discharges. The results indicate the following.

The major radionuclides were ^{99}Mo, ^{65}Ni, ^{58}Co, ^{56}Mn, and ^{51}Cr for the VV, 1 h after shutdown of the NBITF. Total activity dropped slowly because of the dominant nuclide mediate lives: ^{55}Fe ($T_{1/2}$, 2.73 years); ^{51}Cr ($T_{1/2}$, 27.25 days); ^{58}Co ($T_{1/2}$, 70.86 days); and ^{54}Mn ($T_{1/2}$, 312.3 days). For the neutron source calorimeter, the primary nuclides were ^{64}Cu, with a half-life of only 12.7 h. After 1 day of calorimeter, the total activity declined by three orders of magnitude. However, the long-lived nuclides were the main contribution to the shutdown dose rates, and the shutdown dose rates were calculated for different pulse lengths. When the NBITF operated within the design parameters, the maximum value was 4 μSv/h in the perpendicular direction. Following the beamline direction, the highest dose rate was 5.5 μSv/h, which was below the dose-rate limit of IAEA's safety level of 10 μSv/h. As such, maintenance and repair staff can access NBITF after shutdown at a pulse length under 100 s.

Acknowledgments The authors would like to thank the NBI staff for their helpful suggestions on this manuscript.

References

1. S. Sandri, A. Coniglio, M. Pillon et al., Neutron flux and activation calculations for a high current deuteron accelerator, in *2005 IEEE Particle Accelerator Conference*, vol. 1–4 (Knoxville, TN, 2005), pp. 3857–3859
2. G. Martin, A. le Luyer, F. Saint-Laurent, Material activation observations on the tore supra tokamak. Fusion Eng. Des. **58–59**, 973–977 (2001). doi:10.1016/s0920-3796(01)00524-5
3. K. Berkner, W. Cooper, J. McCaslin et al., *Neutron Production in a High-Intensity Deuterium Neutral Beam Facility* (Lawrence Berkeley Lab, California University, Berkeley, 1977)
4. J. Kim, D-d neutron and X-ray yields from high-power deuterium beam injectors. Nucl. Technol. **44**, 315–321 (1979)
5. J. Kim, J.T. Mihalczo, D-d neutron measurements on a 40kv, 60 a neutral beam test facility. Nucl. Instrum. Methods **169**, 83–88 (1980). doi:10.1016/0029-554x(80)90106-8
6. T.T.C. Jones, S.J. Cox, A. Emmanoulidis et al., Prediction of neutron source, tritium production and activation for long-pulse operation of the ITER neutral beam test facility. Nucl. Fusion **46**, S352–S359 (2006). doi:10.1088/0029-5515/46/6/s17
7. K. Nishimura, H. Yamanishi, K. Hayashi et al., Activation analysis for LHD experiments with deuterium gases. Plasma Fusion Res. **3**, S1024–S1024 (2008)
8. Y.X. Chen, Y.C. Wu, Q.Y. Huang, Monte Carlo based operational and shutdown dose rate calculations of HT-7U tokamak. Fusion Eng. Des. **70**, 155–162 (2004). doi:10.1016/j.fusengdes.2003.10.003
9. H.W. Kugel, G. Ascione, C. Tilson et al., Neutron activation cool-down of the tokamak fusion test reactor. Fusion Technol. **34**, 985–990 (1998)
10. M. Brugger, D. Forkel-Wirth, S. Roesler, Generic studies of radioactivity induced by high-energy beams in different absorber materials. Nucl. Technol. **168**, 665–669 (2009)
11. M. Bagatin, A. Coniglio, M. D'Arienzo et al., Radiation environment in the ITER neutral beam injector prototype. IEEE Trans. Nucl. Sci. **59**, 1099–1104 (2012). doi:10.1109/tns.2012.2187461
12. M. Brugger, D. Forkel-Wirth, S. Roesler et al., Studies of induced radioactivity and residual dose rates around beam absorbers of different materials, in *Beam Material Interaction, Proceedings of HB* (2010), pp. 448–452
13. J.-Q. Xu, X.-B. Xia, Y.-X.-Z. Sheng et al., Dose rate distribution of photoneutrons in an id beamline of SSRF: simulations and measurements. Nucl. Sci. Tech. **25**, 050101 (2014). doi:10.13538/j.1001-8042/nst.25.050101
14. G. Battistoni, F. Broggi, M. Brugger, The application of the Monte Carlo code FLUKA in radiation protection studies for the large Hadron collider. Prog. Nucl. Sci. Technol. **2**, 358–364 (2011)
15. C. Hu, NBI Team, Conceptual design of neutral beam injection system for east. Plasma Sci. Technol. (2012). doi:10.1088/1009-0630/14/6/30
16. Y.Q. Chen, B. Wu, J.F. Wang et al., Analysis of fusion neutron production in east with neutral beam injection. Nucl. Tech. **36**, 110603 (2013). **(in Chinese)**

17. L.X. Liu, B. Xiao, Y.X.Z. Sheng et al., Effects of scattered neutrons on the neutron radiation field generated by Cf-252 neutron source with a shield. Nucl. Tech. **36**, 100201 (2013). **(in Chinese)**
18. S.H. Tian, H. Wang, X. Chen et al., Simulation and verification of neutron scattering at 252cf (d2o) neutron laboratory. Nucl. Tech. **37**, 060204 (2014). doi:10.11889/j.0253-3219.2014.hjs.37.060204. **(in Chinese)**
19. C.X. Zhu, Y.F. Mou, P. Zheng, (n, γ)Discrimination and distribution of neutron capture time measurement of gadolinium-loaded liquid scintillator. Nucl. Tech. **37**, 110404 (2014). doi:10.11889/j.0253-3219.2014.hjs.37.110404. **(in Chinese)**
20. M.M. Rehani, Training of interventional cardiologists in radiation protection—the iaea's initiatives. Int. J. Cardiol. **114**, 256–260 (2007)